Electronic Supplementary Material (ESI) for Energy & Environmental Science.

Supporting Information

Organic iodides in efficient and stable perovskite solar cells: strong surface passivation and interaction

Guanhua Ren [#a], Zhiguo Zhang [#b], Yanyu Deng[a], Zhuowei Li [a], Chunyu Liu[*a], Mingkui Wang[*b], and Wenbin Guo [*a]

[a] *State Key Laboratory of Integrated Optoelectronics, College of Electronic Science and Engineering, Jilin University, 2699 Qianjin Street, Changchun 130012, People's Republic of China*

[b] *Wuhan National Laboratory for Optoelectronics, Huazhong University of Science and Technology, 1037 Luoyu Road, Wuhan 430074, Hubei, P. R. China*

Experimental Section

Materials:

The SnO_2 (15% in H_2O colloidal dispersion) was purchased from Alfa Aesar. The lead iodide (PbI_2, >99.99%), formamidinium iodide (FAI, ≥99.5%), methyfammonium iodide (MAI, ≥99.5%), methylammonium chloride (MACl, >99.5%), spiro-OMeTAD (≥99.8%), poly[bis(4-phenyl)(2,4,6-trimethylphenyl)amine] (PTAA), LiTFSI (>99%), TBP (>96%), PMAI (≥99.5%), PEAI (≥99.5%), PPAI (≥99.5%) and PBAI (≥99.5%) were obtained from Xi'an Polymer Light Technology Corp in China. The N,N-dimethylformamide (DMF, 99.9%), dimethyl sulfoxide (DMSO, 99%) and chlorobenzene (CB, 99.8%) were obtained from J&K Scientific. The isopropanol (IPA, ≥99.7%) was purchased from Sinopharm Chemical Reagent Co. Ltd.

Device Fabrication:

The ITO-coated glass substrates were cleaned by deionized water, acetone and IPA in an ultrasonic machine for 20 min and dried by N_2 blow. Then these substrates were treated with UV-zone for 20 min. The SnO_2 precursor (SnO_2:H_2O=1:4 (V/V)) was spin coated on the substrate at 3000 rpm for 30 s following with annealling at 150 °C for 20 min to obtain the SnO_2 electron transport layer. The PbI_2 (1.5 mmol) was dissolved in 1 mL DMF and DMSO (V/V=9:1) and then spin coated onto cooled SnO_2 at 2000 rpm for 30 s following with annealling at 70 °C for 1 min. Subsequently, 100 μL of organic mixture solution of FAI:MAI:MACl (90 mg:6.39 mg:9 mg in 1 mL IPA) was spin coated onto the PbI_2 film at 2000 rpm for 30 s. After the resulting films turned dark orange in the glove box, they were thermally annealed at 150 °C for 30 min in 30-40% RH condition to form $FA_{1-x}MA_xPbI_3$ perovskite films. For the control perovskite film, 50 μL of IPA was dynamically spin coated on the perovskites at 4000 rpm for 30 s. For the surface treatment by I_2 in IPA, solid I_2 was dissolved in IPA and stirred at 80°C for 7 days, the concentrations are identified from the concentration of atomic iodine, as previously reported.[1, 2] For the surface treatment by PA iodides, 50 μL of PMAI, PEAI, PPAI and PBAI solutions (12 mM, 20 mM and 30 mM in IPA) were dynamically spin coated on the perovskites at 4000 rpm for 30 s, respectively. The spiro-OMeTAD solution was prepared by dissolving 72.3 mg of spiro-OMeTAD, 17.6 μL of LiTFSI solution (520 mg /mL in acetonitrile) and 28.5 μL TBP in 1 mL CB. Next, the spiro-OMeTAD solution was deposited at 4000 rpm for 30 s as the HTL. After that, they were placed in a drying tower for 20 h to complete the oxidation. Fig. S23 shows the photographs of the drying tower and detection of the temperature and humidity inside the tower. Prior to placing the samples in the drying tower, the ambient humidity was controlled to below 30% using a dehumidifier. Then the samples and a temperature and humidity meter are placed in the drying tower and petroleum jelly is applied evenly to the interface to enhance the seal ability. The temperature and humidity meter is connected to a phone for real-time detection. The color-changing silica gel is placed at the bottom of the drying tower to reduce the humidity inside the tower. The humidity inside the drying tower drops from ambient humidity to less than 10%, which takes about 3 h. During the remaining 17 h, the humidity inside the drying tower was kept below 10% and the temperature was between 20-25°C. Finally, 8 nm-thick of MoO_3 and 100 nm-thick of Ag electrode was deposited in a vacuum condition ($<10^{-4}$ pa). The devices were completed and the effective area is 0.044 cm^2. In photothremal stability measurment, spiro-OMeTAD was replced by PTAA to exclude the effect of spiro-OMeTAD failure at high temperature.[3, 4]

Characterizations:

J-V: The J-V curves were measured using a Keithley 2400 source meter under AM 1.5G solar illumination. The dark J-V curves were measured a Keithley 2400 source meter in the dark condition.

PAS: The measurement of PAS was entrusted to “eceshi” testing institution (www.eceshi.com). The positrons emitted by ^{22}Na are incident into the sample and annihilate with the electrons therein, emitting γ rays. The 1.27 MeV γ photon marks the production of a positron and serves as the starting signal, and a 511 keV annihilation radiation γ photon serves as a termination signal, and the time between the two signals is the lifetime. Two identical samples are required for each measurment. The data are analyzed by the PATFIT software to obtain the lifetime (τ) and relative intensity (I) of the samples.

XPS: XPS was conducted on a Thermo Scientific ESCALANTM 250Xi system. The sample size was 0.5 cm × 0.5 cm. The measurement was conducted in a high vacuum environment. X-ray photons were emitted from a monochromatic Al Kα source. The total acquisition time of high-resolution spectrum for each element was less than 3 min. The number of scans was 5. The X-ray spot size was 400 μm. The lens mode was standard mode and the analyser mode was CAE: Pass Energy 50.0 eV. The energy step size was 0.050 eV and the number of energy steps was 401. The obtained spectra were analyzed with the Avantage software.

Ultraviolet photoelectron spectroscopy (UPS): UPS was conducted on a Thermo Scientific ESCALANTM 250Xi system. The sample size was 1.5 cm × 1.5 cm. The measurement was conducted in a high vacuum environment. The photons with low energy were emitted from a He I source. The total acquisition time for each sample was about 1 min. The number of scans was 2. The lens mode was UPS mode and the analyser mode was CAE: Pass Energy 4.0 eV. The energy step size was 0.050 eV and the number of energy steps was 581. UPS measurements were calibrated using an Au sample. Importantly, the surface of the sample needs to be evenly distributed and cleaned.

TAS: The TAS of the PSCs were characterized at 263 K, 270 K, 285 K and 300 K using a Precision Impedance Analyzer 6500B Series of Wayne Kerr Electronics. First, the PSCs were encapsulated (see details in the Results and Discussion). Next, they were placed in the device equipped with dual-probe measurement and temperature detection systems. The vacuum level was adjusted to below 10^{-2} pa using a mechanical pump. Liquid nitrogen was introduced and the flow rate was adjusted to slowly reduce the temperature. The precision impedance analyzer and dual-probe measurement were connected. Open circuit calibration, short circuit calibration and high-frequency calibration of the precision impedance analyzer were performed before measuring TAS spectra. The frequency range was 20 to 20 M Hz. The input drive voltage was 0.1 V.

E_a: The E_a values are obtained from fitting the Arrhenius plots using the equation[5, 6]

$$\omega_{peak} = \beta T^2 \exp\left(-\frac{E_a}{k_B T}\right) \tag{1}$$

where ω_{peak} is the value of characteristic transition frequency, β is the temperature-related factor, T is the temperature, k_B is the Boltzmann constant.

IPCE: The IPCE spectra were measured with a Crowntech QTest Station 1000 AD. The measurement range was 300-850 nm. The incident slit, exit slit and intermediate slit were 3.0 mm, 3.0 mm and 1.0 mm, respectively. The specified wavelength was 550 nm. The standard silicon photovoltaic cell was used as the standard sample.

Importantly, the light spot should be completely focused on the device.

XRD: The XRD patterns of the perovskite films were measured on a Shimadzu XRD-6000 diffractometer with Cu Kα radiation. The operation voltage and current were 40 kV and 200 mA, respectively. All samples were kept at the same height. The scan range was 1-40 degree. The scan speed was 15.00 degree/min. The measurement was conducted in the air condition at room temperature.

SEM: The cross-sectional and surface SEM images were characterized using a JEOL JSM-7500F field-emission SEM. The samples were fixed to the aluminum column with conductive tape. A thin Pt layer was deposited on the sample surface to enhance conductivity. The measurement was conducted in a high vacuum environment ($<5\times10^{-4}$ pa). The acceleration voltage was 5 kV. The magnification of surface SEM images was 20000 times.

Absorption spectra: The absorption spectra of the perovskite films were performed with UV 1700 photometer, Shimadzu. The perovskite films were deposited on the ITO/SnO_2 substrate. The measurement range was 600-900 nm and the ITO/SnO_2 substrate was used as baseline.

PL: The PL spectra was conducted on a Shimadzu RF 5301 fluorescence spectrophotometer. The perovskite films were deposited on the ITO substrate. The wavelength of excitation light is 532 nm.

SCLC: The I-V curves of SCLC measurements were obtained by a Keithley 2400 source meter in dark condition. N_t can be estimated by the formula[7]

$$N_t = \frac{2\varepsilon_0\varepsilon_r V_{TFL}}{qL^2} \tag{2}$$

in which ε_0 is the vacuum permittivity, ε_r is the relative dielectric constant, V_{TFL} is the trap-filled limit voltage, q is the elemental charge, and L is the thickness of the perovskite film.

tDOS: The tDOS of the PSCs were derived from angle frequency-dependent capacitance (C-ω) data. The C-ω curves were characterized using a Precision Impedance Analyzer 6500B Series of Wayne Kerr Electronics. Open circuit calibration, short circuit calibration and high-frequency calibration of the precision impedance analyzer were performed before measuring the C-ω curves. The frequency range was 20 to 20 M Hz. The input drive voltage was reduced to the minimum value (10 mV). The tDOS was calculated using the equation[8, 9]

$$tDOS(E_\omega) = -\frac{dC}{d\omega}\frac{V}{qW}\frac{\omega}{k_BT} \tag{3}$$

where C is the capacitance, ω is the angular frequency, V is the applied bias voltage, q is the elementary charge, W is the thickness of the perovskite layer, k_B is the Boltzmann constant, and T is the temperature. The E_ω was calculated by the equation[10]

$$E_{\omega} = k_B T ln(\frac{\omega_0}{\omega}) \tag{4}$$

where ω_0 is the attempt-to-escape frequency.

EIS: The impedance spectroscopy were obtained using a Precision Impedance Analyzer 6500B Series of Wayne Kerr Electronics. Open circuit calibration, short circuit calibration and high-frequency calibration of the precision impedance analyzer were performed before measuring the curves. The frequency range was 20 to 20 M Hz. The input drive voltage was 0.1 V.

DFT simulation:

The first principles computations were carried out by Vienna Ab initio Simulation Package (VASP) based on density functional theory. Generalized gradient approximation (GGA) with the Perdew-Burke-Ernzerhof (PBE) functional was used to describe the exchange-correlation interaction. The projector augmented wave pseudopotentials were adopted to describe the ion-electron with a cutoff energy of 450 eV. The K-point grid of Brillouin zone was tested and sampled by 3×3×1 within Gamma-Pack. The electronic energy and forces were converged to within 10^{-5} eV and 0.03 eVÅ^{-1}, respectively. The vacuum layer in the slab model is larger than 15 Å to avoid superficial interaction between periodical slabs. In order to calculate the adsorption energy of passivator on perovskite surface, the following expression was used: $E_b = E_{surf + passivator} - E_{surf} - E_{passivator}$, where $E_{surf + passivator}$, E_{surf}, and $E_{passivator}$ are the total energies of the surface with passivator, the clean surface, and the passivator, respectively.[11] Three acceptor-like defects V_{FA}, V_{Pb} and I_{Pb} are considered. The electrostatic potentials (φ) of the passivators were calculated using the Gaussian 09 package at the B3LYP/def2TZVP level with DFT-D3.

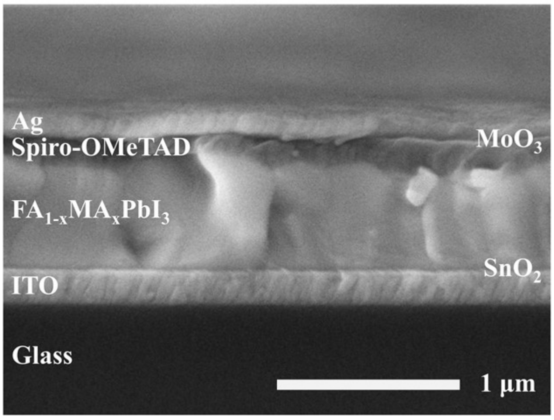

Fig. S1. The cross-sectional SEM image of the fabricated PSCs.

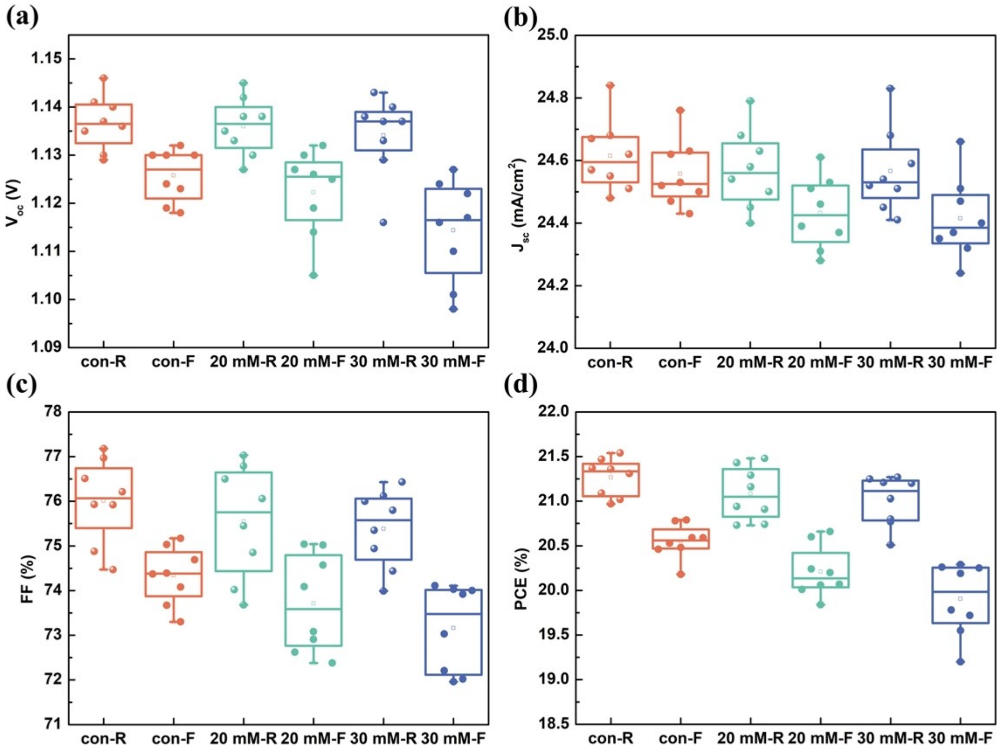

Fig. S2. Distribution of (a) V_{oc}, (b) J_{sc}, (c) FF and (d) PCE of the control and treated devices. Here "con" represents the control device, "R" and "F" means reverse and forward scan, respecively. 8 individual cells are considered for each device type.

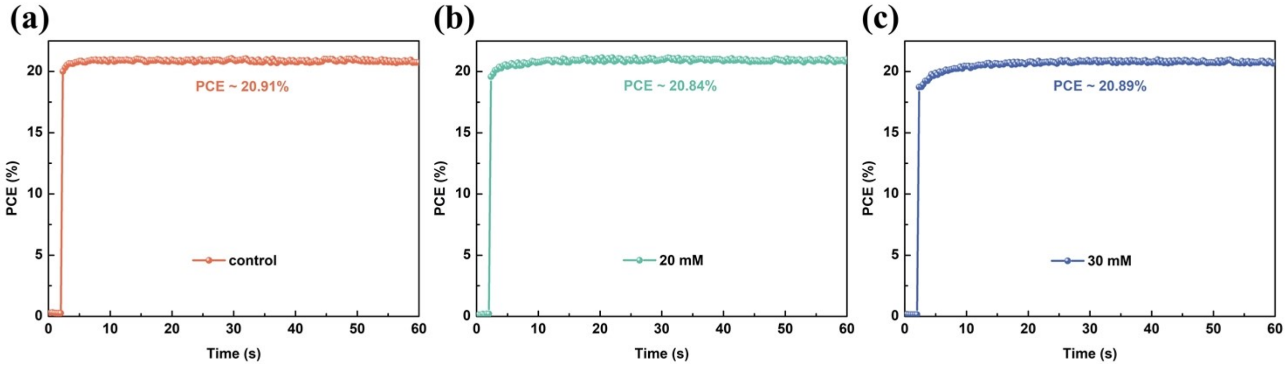

Fig. S3. Stabilized PCEs of the control and treated devices.

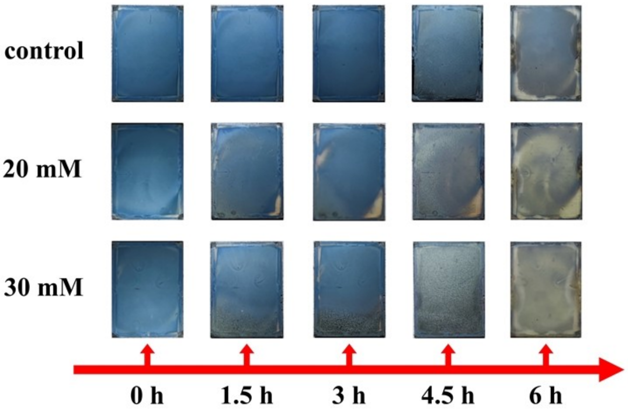

Fig. S4. Photographs of the evolution of perovskite films in I_2 vapor.

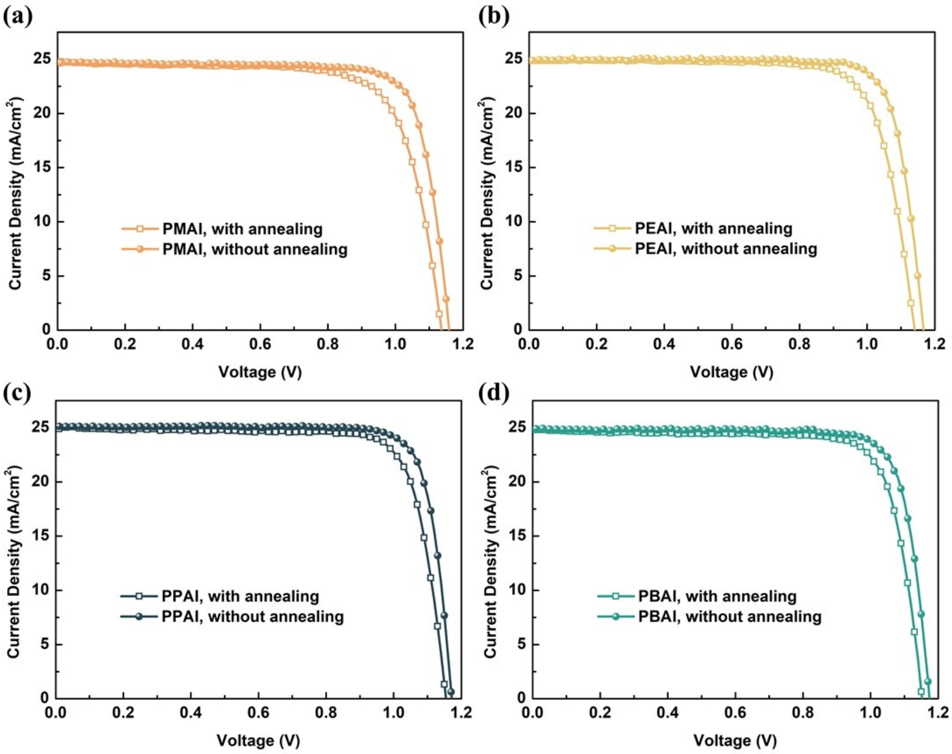

Fig. S5. J-V curves of the devices (12 mM) with or without annealing. The annealing temperature and time are 100°C and 3 min, respectively.

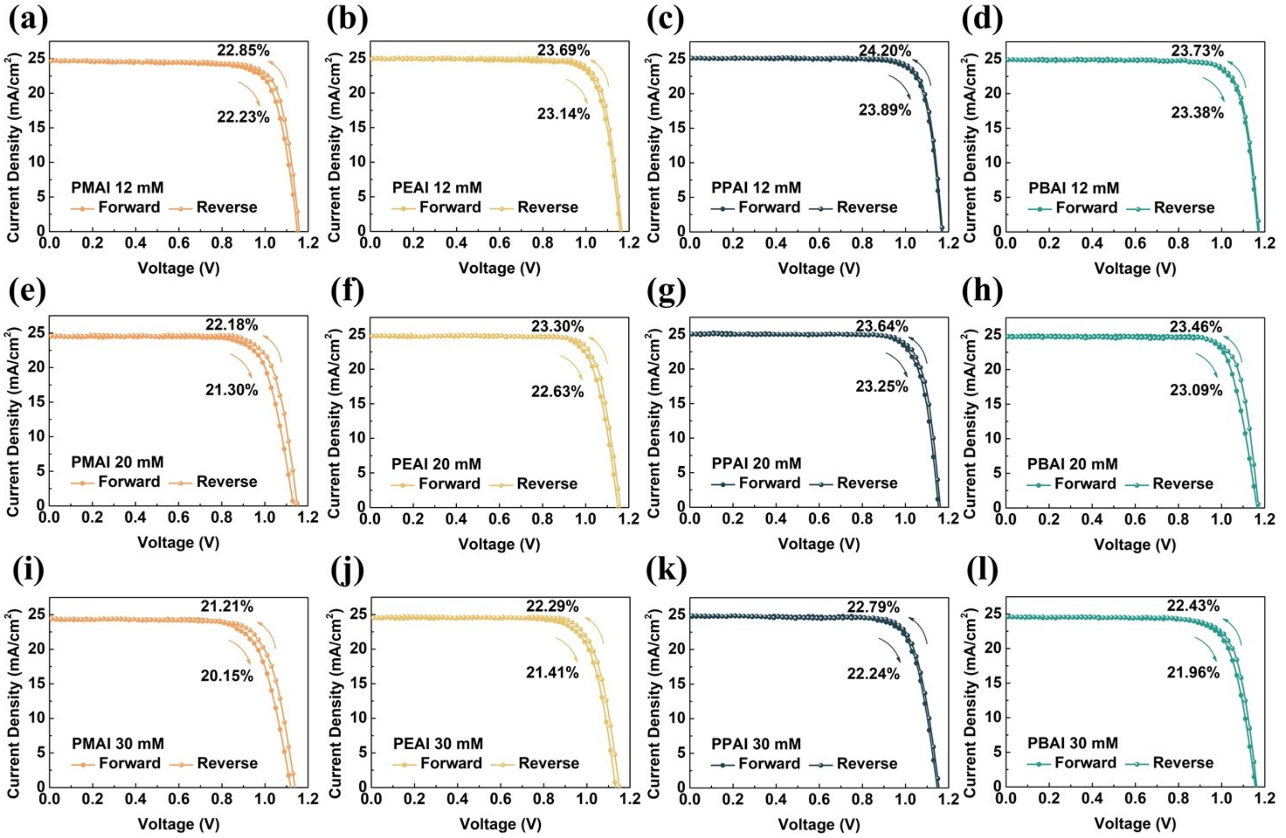

Fig. S6. J-V curves of the devices treated with diffrenent concerntrations of PA iodides, including reverse and forward scans.

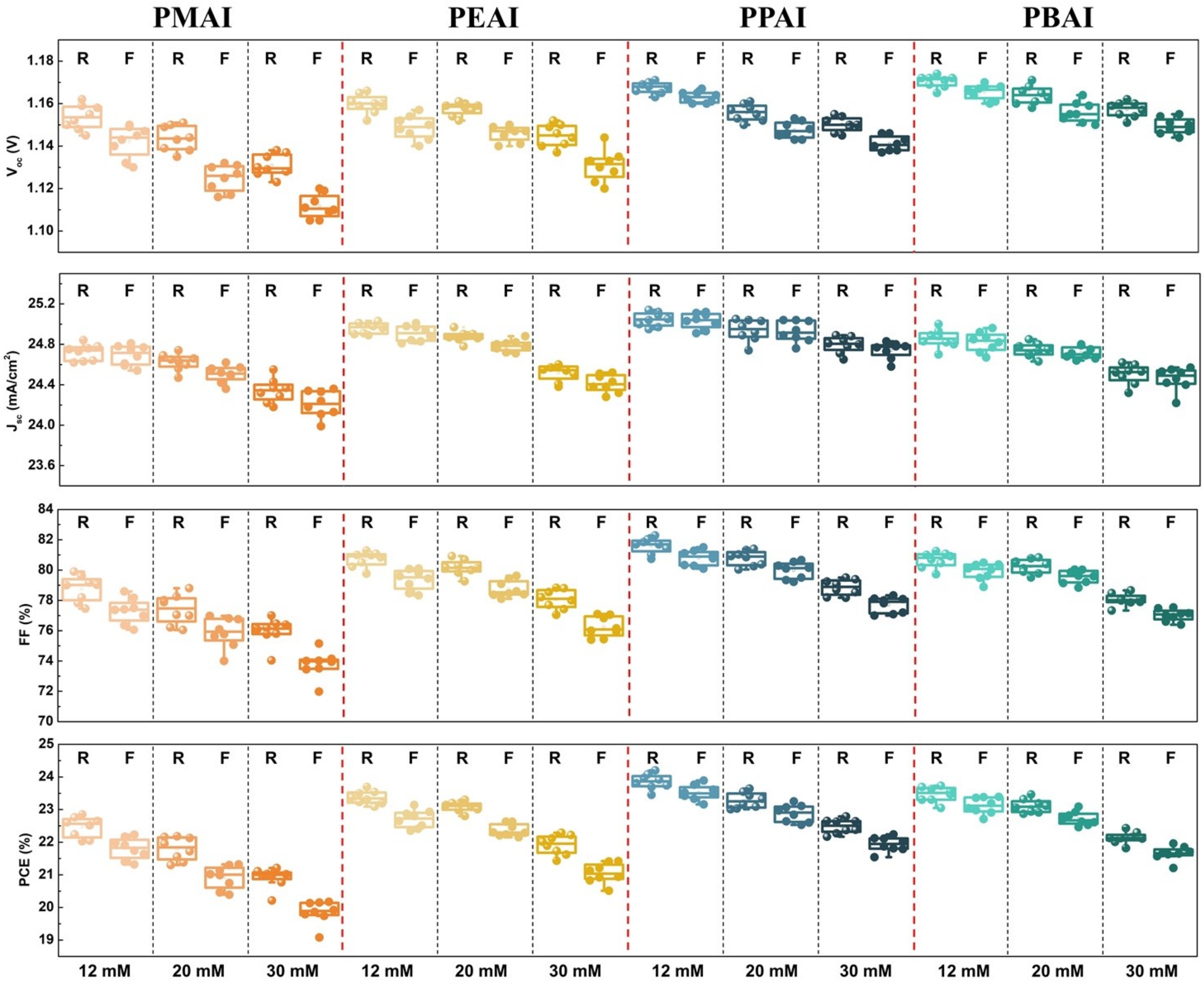

Fig. S7. Distribution of (a) V_{oc}, (b) J_{sc}, (c) FF and (d) PCE of the devices treated with diffenent concerntrations of PA iodides. “R” and “F” means reverse and forward scan, respecively. 8 individual cells are considered for each device type.

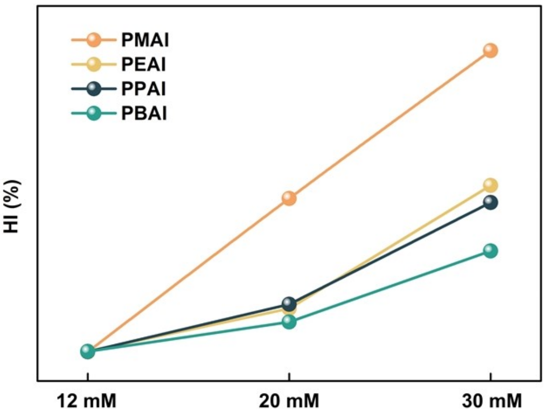

Fig. S8. The change of the mean of HI with concentration.

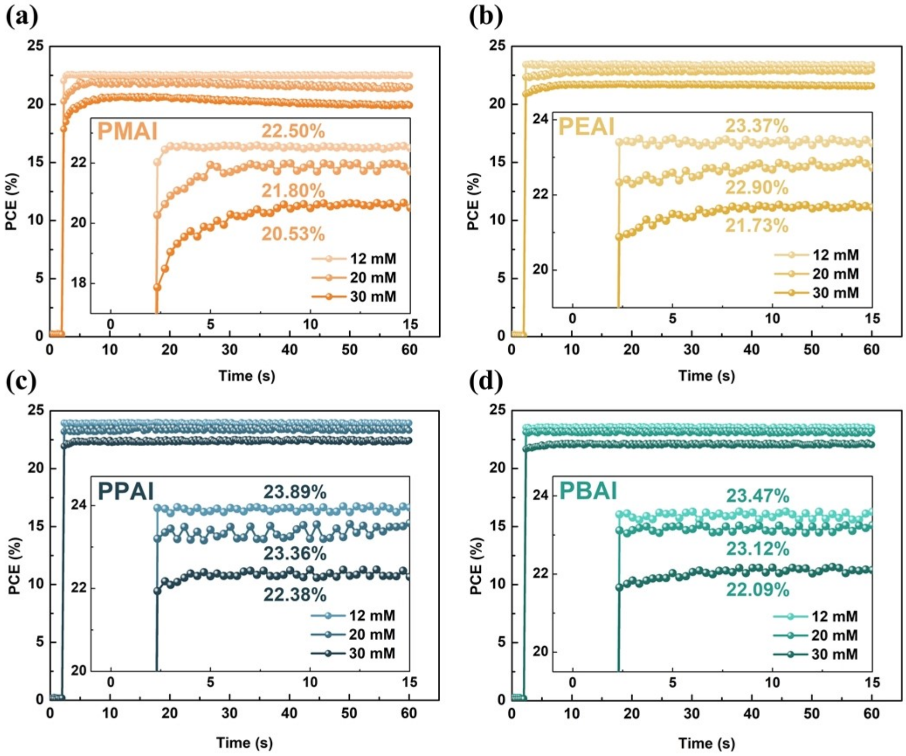

Fig. S9. Stabilized PCEs of the devices treated with different concentrations of PA iodides.

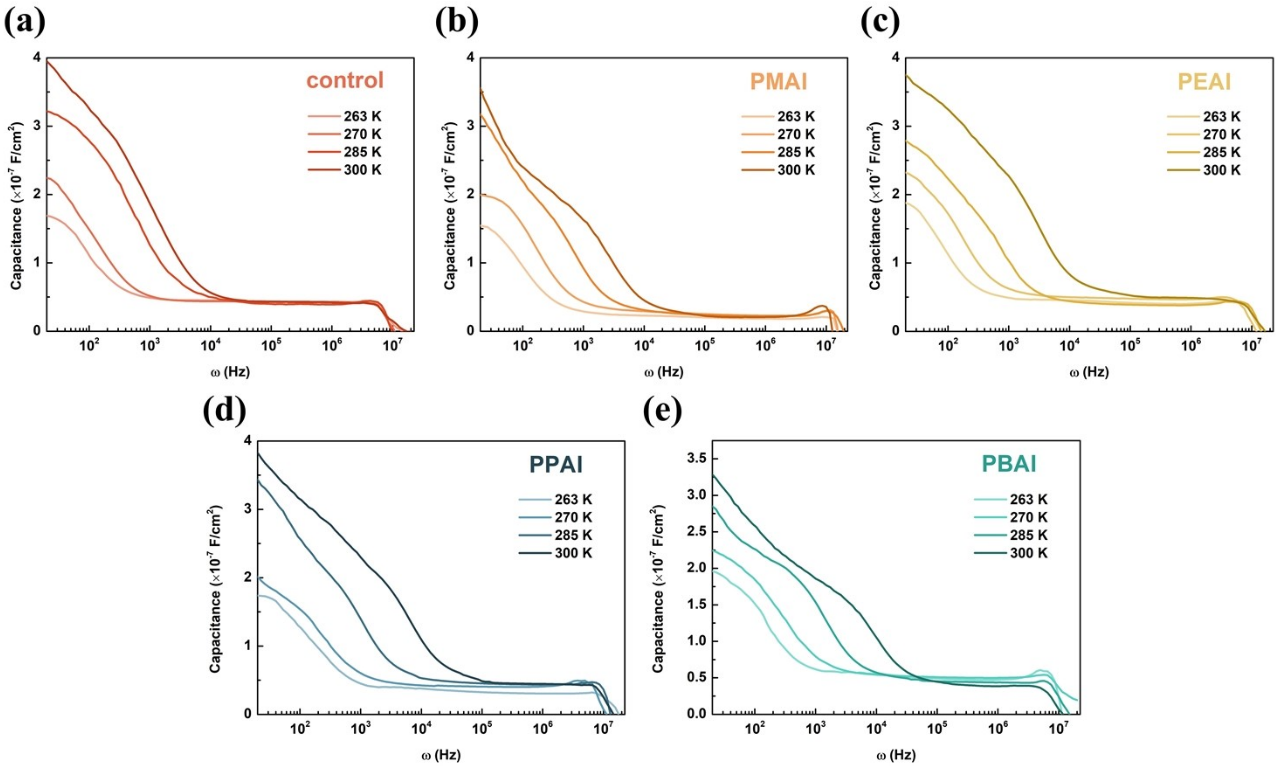

Fig. S10. The TAS spectra of the (a) control, (b) PMAI-treated, (c) PEAI-treated, (d) PPAI-treated and (e) PBAI-treated devices measured at different temperatures.

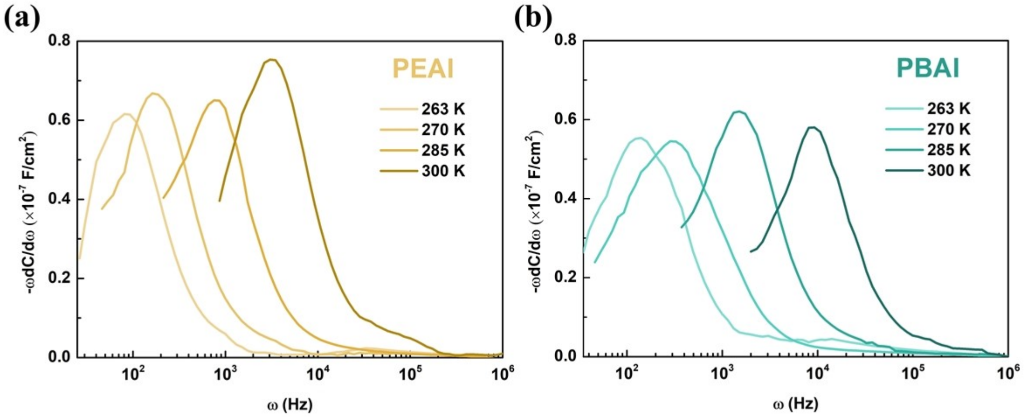

Fig. S11. The -ωdC/dω versus ω spectra of the (a) PEAI and (b) PBAI-treated devices measured at different temperatures. Part of the data to the left of each characteristic peak are not given for improving data visualization.

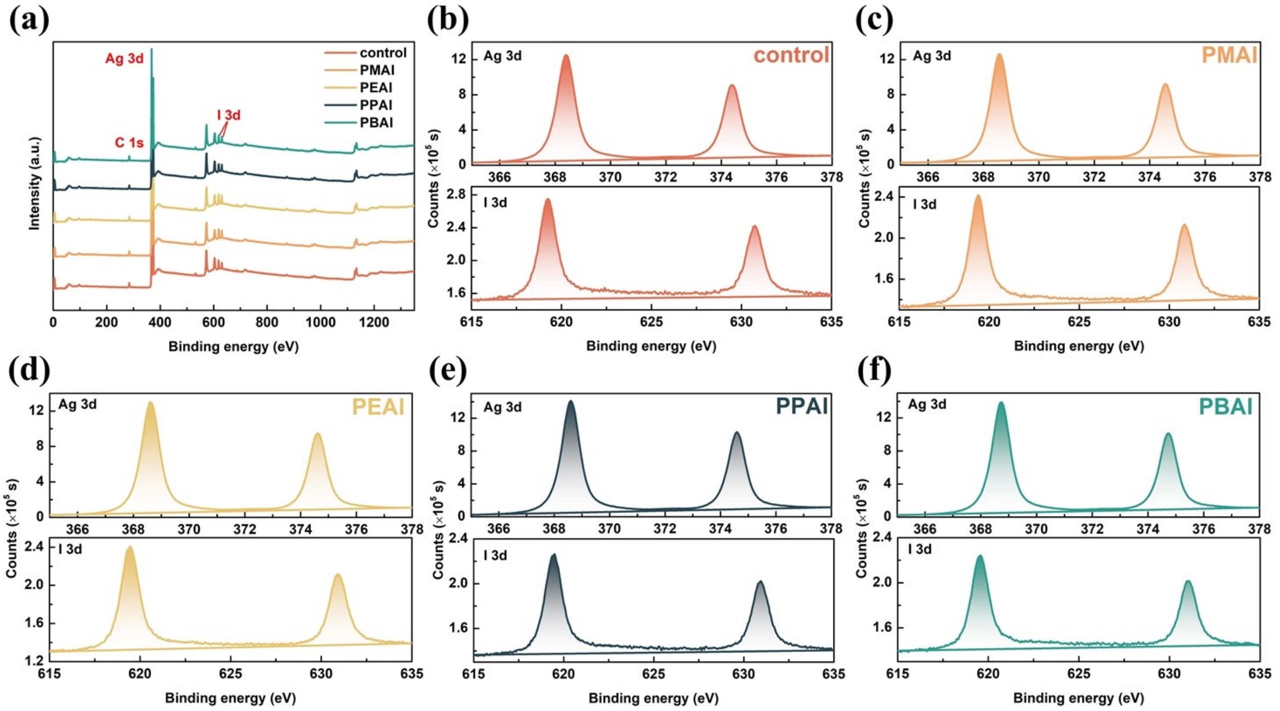

Fig. S12. (a) XPS survey of Ag electrode surface of the aged devices. (b)-(f) High-resolution XPS spectra depicting the Ag 3d and I 3d peaks of Ag electrode surface of the aged devices.

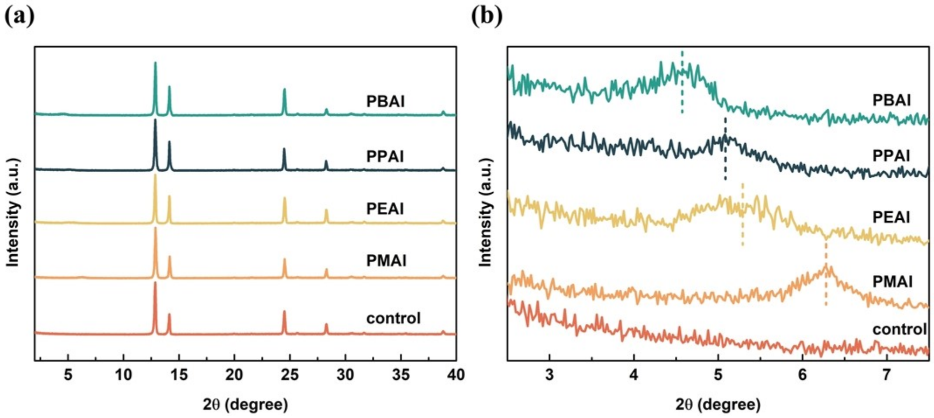

Fig. S13. XRD patterns of the control and PA-iodides-treated perovskite films in (a) 2-40° region and (b) 2.5-7.5° region.

Although the perovskite films are not annealed after PA iodides treatment, the signals of low-dimensional perovskites are observed (marked with vertical dashed lines in Fig. S13b),[12] indicating that the transformation of low-dimensional perovskites still occurs even at room temperature.

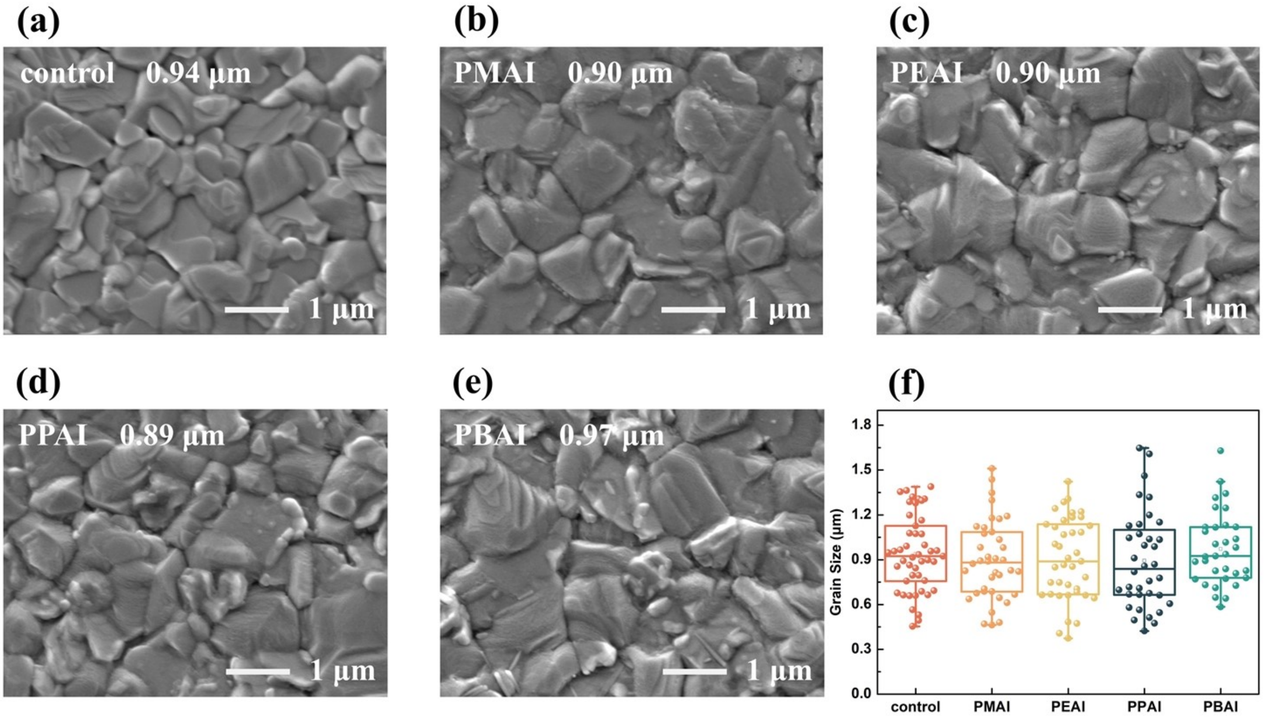

Fig. S14. SEM images of the (a) control, (b) PMAI-treated, (c) PEAI-treated, (d) PPAI-treated and (e) PBAI-treated perovskite films. The average grain size is marked on top of the image. (f) The grain size statistics of these perovskite films, with the number of grains ranging from 30 to 50.

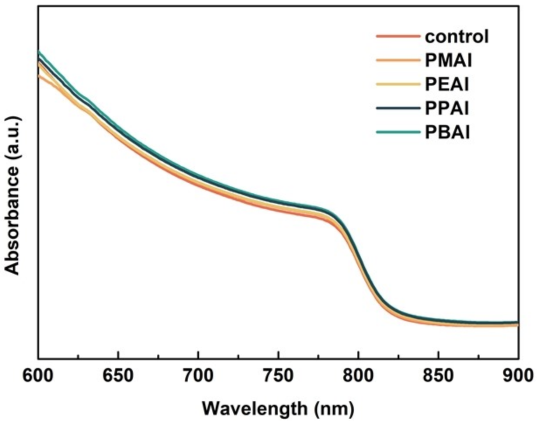

Fig. S15. Absorption spectra of the perovskite film treated with differnet PA iodides.

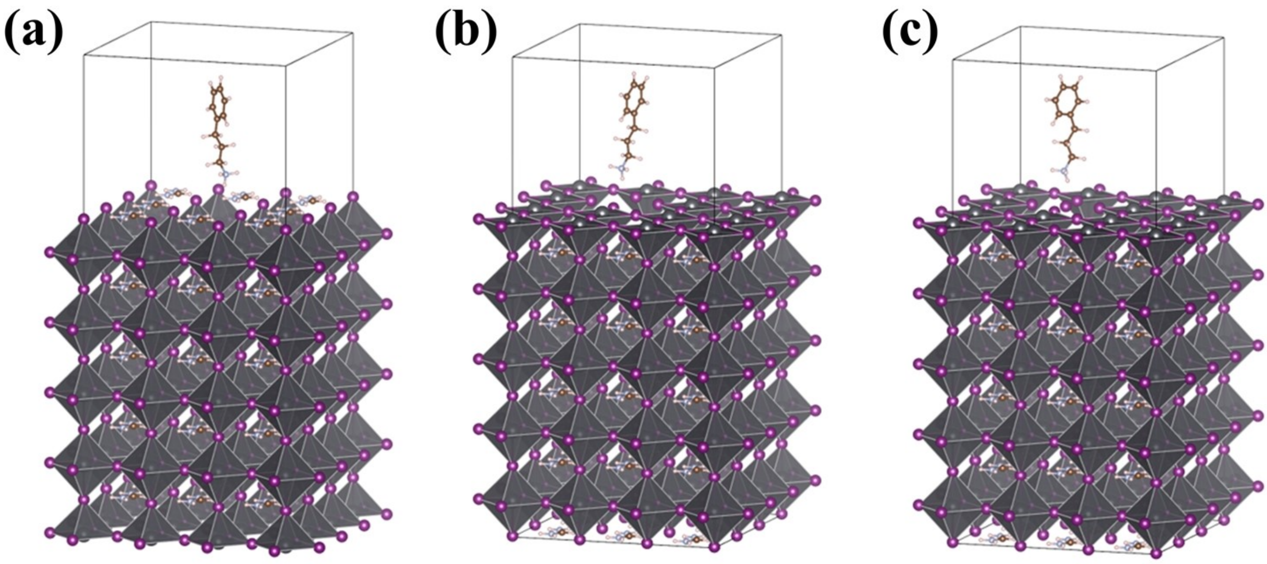

Fig. S16. Schematic diagram of the interaction between PA cations (using PPA as the example) with (a) V_{FA}, (b) V_{Pb} and (c) I_{Pb} defects.

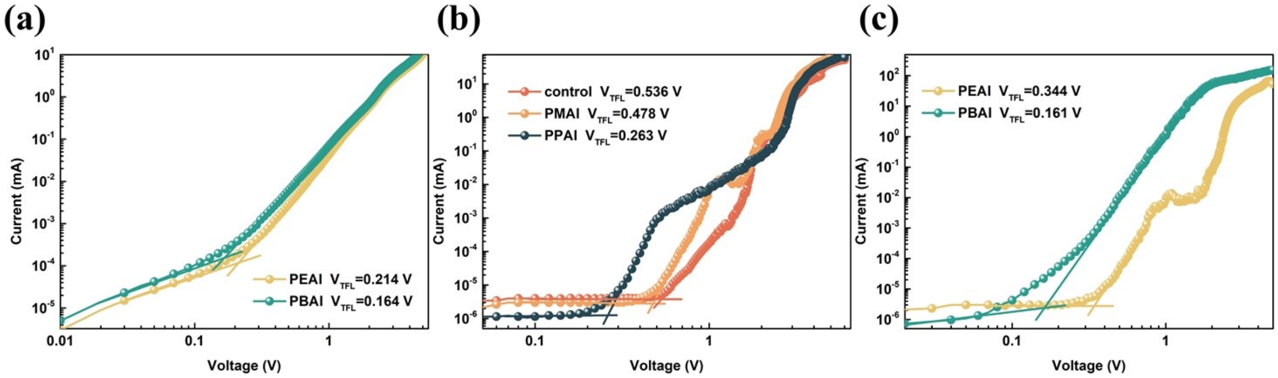

Fig. S17. (a) The I-V curves of the hole only PEAI-treated and PBAI-treated devices. (b)-(c) The I-V curves of the electron only devices.

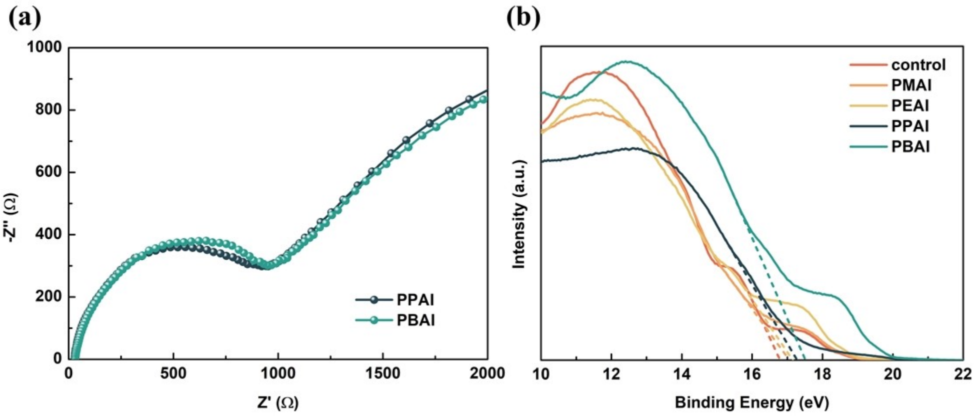

Fig. S18. (a) Nyquist plots of the PPAI-treated and PBAI-treated devices. (b) UPS spectra of the secondary-electron cut-off region of the devices.

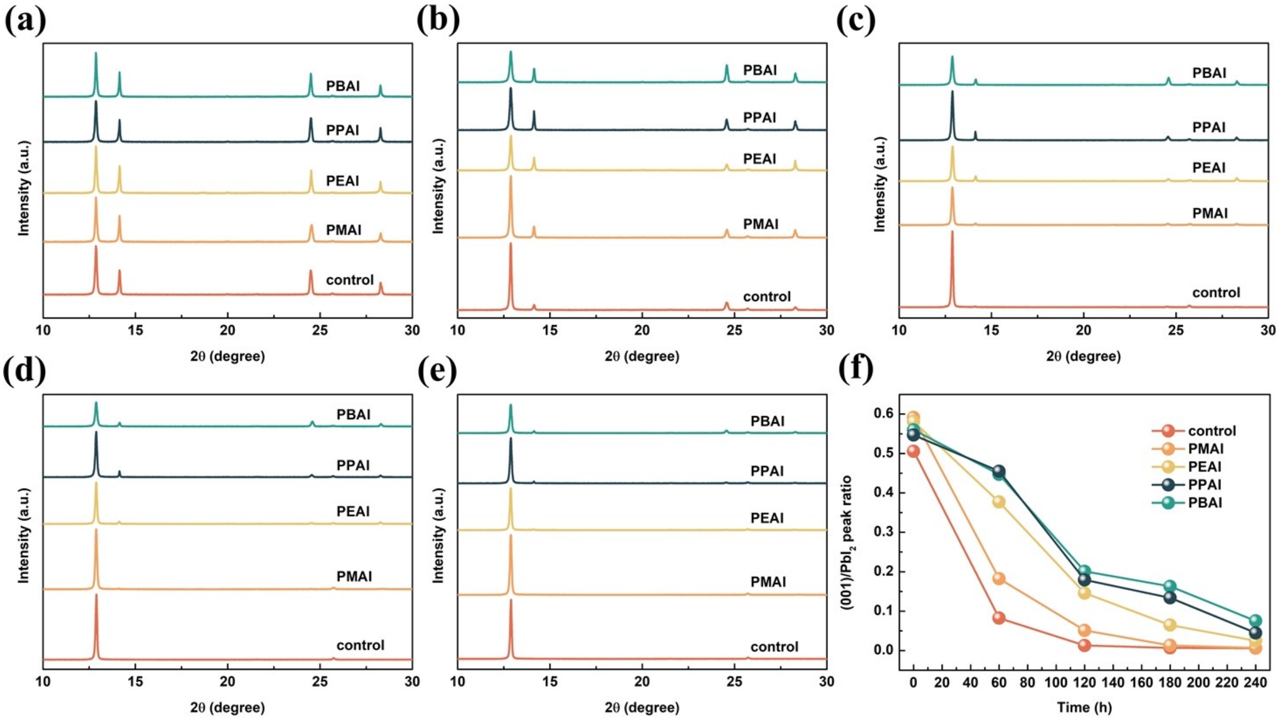

Fig. S19. (a)-(e) The XRD patterns evolution of different perovskite films as a function of time (continuous illumination at 85°C in N_2). The time interval is 60 h. (f) (001)/PbI_2 peak ratio of the different films as the function of time.

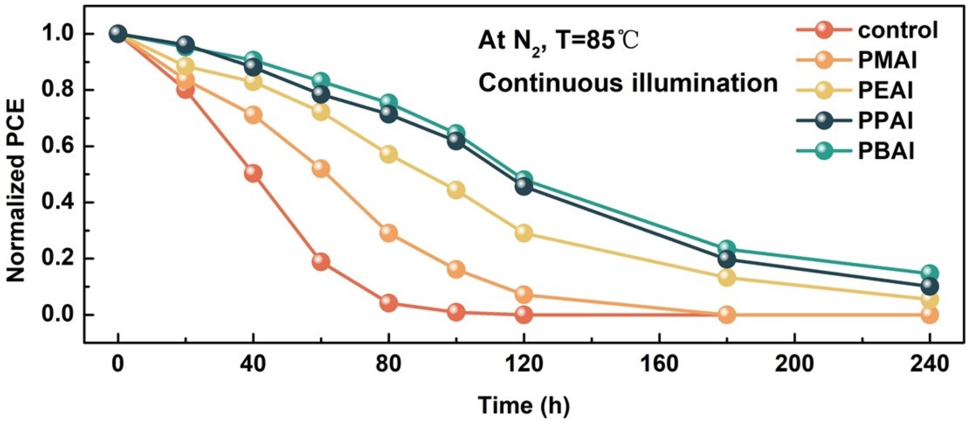

Fig. S20. Photothermal stability of the devices under continuous illumination (Xenon lamp, simulated 1 sun illumination) at 85°C in N_2 atmosphere. 3 individual cells are considered for each device type, and the average of these three device PCEs is used as the result.

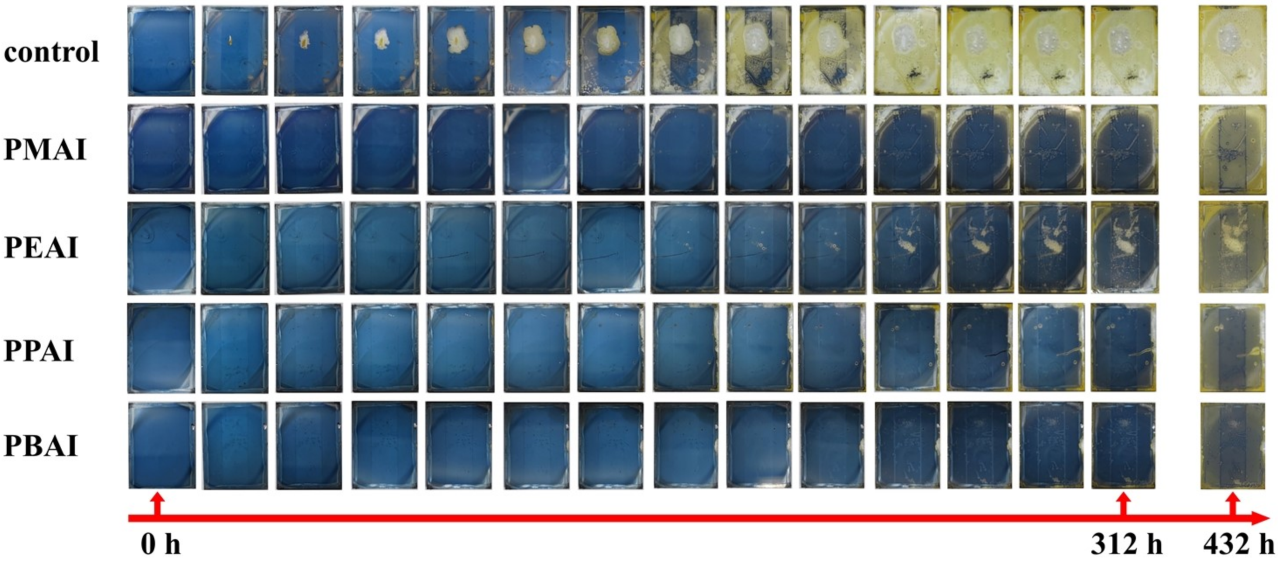

Fig. S21. Photographs of the evolution of perovskite films in the condition of about 85% RH at room temperature. The time interval is 24 h.

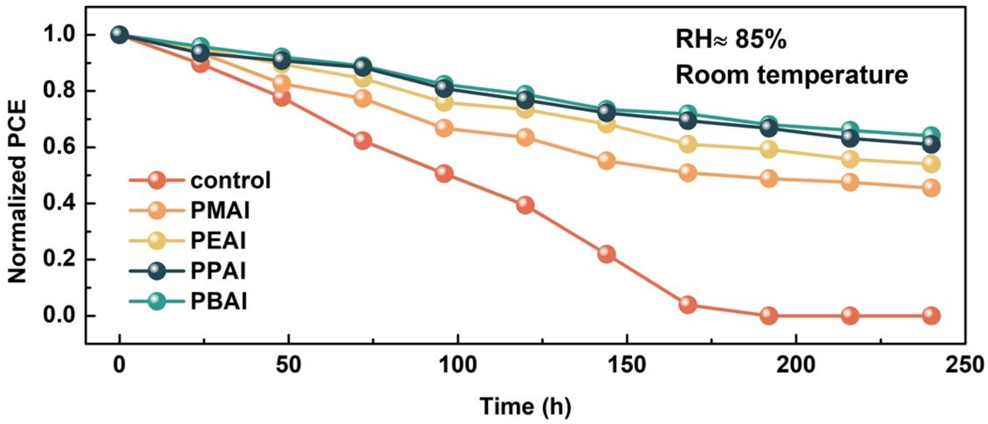

Fig. S22. Humidity stability of the unencapsulated devices in the condition of 85% RH at room temperature. 3 individual cells are considered for each device type, and the average of these three device PCEs is used as the result.

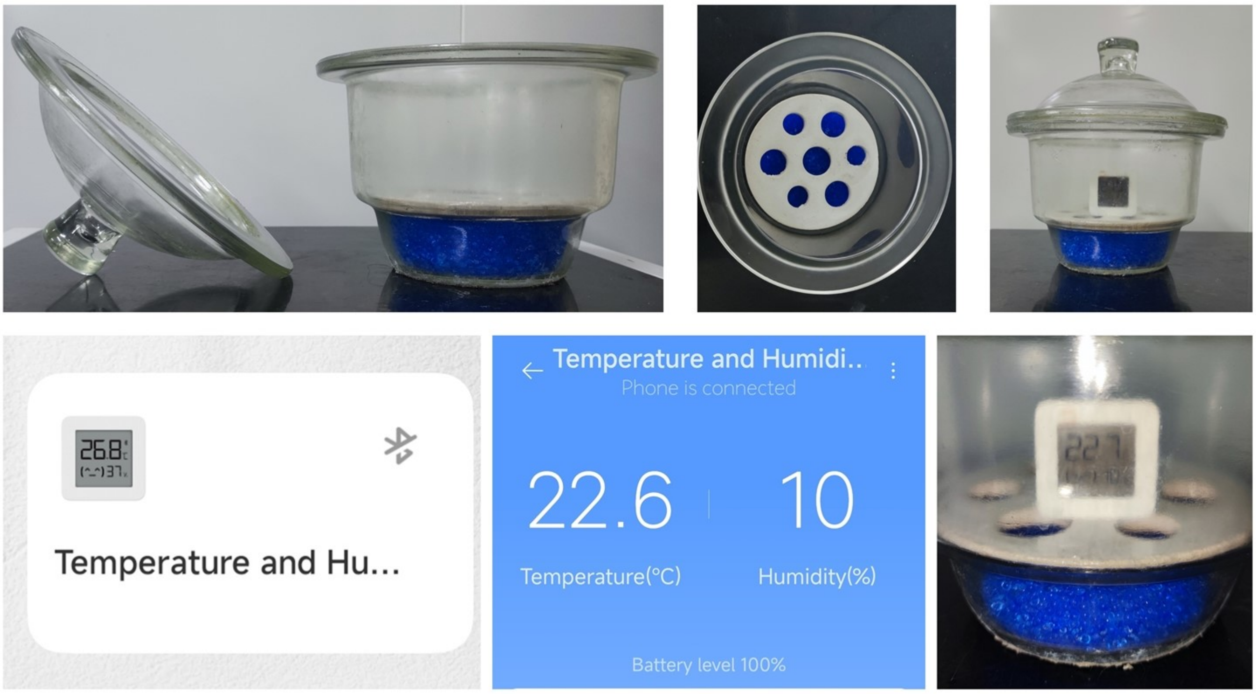

Fig. S23. The photographs of the drying tower and detection of the temperature and humidity inside the tower.

Table S1. Photovoltaic parameters of the control and treated PSCs. 8 individual cells are considered for each device type.

Device		Scanning direction	V_{oc} (V)	J_{sc} (mA/cm^2)	FF (%)	PCE (%)	HI (%)
control	best	reverse	1.140	24.55	76.97	21.54	3.48
		forward	1.132	24.43	75.17	20.79	
	average	reverse	1.137	24.62	76.00	21.27	3.37
		forward	1.126	24.56	74.34	20.56	
20 mM	best	reverse	1.138	24.58	76.79	21.48	3.82
		forward	1.126	24.46	75.02	20.66	
	average	reverse	1.136	24.57	75.55	21.09	4.15
		forward	1.122	24.43	73.71	20.20	
30 mM	best	reverse	1.140	24.51	76.12	21.27	4.61
		forward	1.127	24.32	74.03	20.29	
	average	reverse	1.134	24.57	75.38	21.00	5.24
		forward	1.114	24.42	73.16	19.90	

Table S2. Positron lifetime parameters of the control and treated films.

Sample	τ_1 (ps)	τ_2 (ps)	τ_3 (ps)	I_1 (%)	I_2 (%)	I_3 (%)
control-1	168.3	382.6	978.0	12.96	64.50	22.54
control-2	167.6	376.9	987.6	11.49	66.17	22.34
20 mM-1	162.5	385.2	975.4	12.53	64.45	23.02
20 mM-2	160.6	386.9	987.6	12.22	64.79	22.99
30 mM-1	160.7	393.2	1020.3	15.34	64.33	20.33
30 mM-2	160.5	390.4	1039.2	16.25	64.68	19.07

Table S3. Photovoltaic parameters of the champion devices (12 mM) with or without annealing.

Device	Annealing	V_{oc} (V)	J_{sc} (mA/cm^2)	FF (%)	PCE (%)
PMAI	with	1.136	24.70	74.55	20.92
	without	1.159	24.76	79.61	22.85
PEAI	with	1.140	24.91	77.37	21.97
	without	1.166	25.00	81.28	23.69
PPAI	with	1.154	25.01	79.52	22.95
	without	1.171	25.12	82.28	24.20
PBAI	with	1.152	24.80	79.03	22.58
	without	1.174	24.88	81.25	23.73

Table S4. The average of photovoltaic parameters of the champion devices treated with diffrenent concerntrations of PA iodides. 8 individual cells are considered for each device type.

Device	Concentration	Scanning direction	V_{oc} (V)	J_{sc} (mA/cm^2)	FF (%)	PCE (%)	HI (%)
PMAI	12 mM	reverse	1.154	24.72	78.77	22.47	2.96
		forward	1.142	24.69	77.31	21.80	
	20 mM	reverse	1.144	24.63	77.41	21.81	4.03
		forward	1.125	24.51	75.89	20.93	
	30 mM	reverse	1.131	24.34	75.97	20.91	5.06
		forward	1.112	24.21	73.78	19.86	
PEAI	12 mM	reverse	1.160	24.96	80.71	23.37	2.82
		forward	1.149	24.91	79.36	22.71	
	20 mM	reverse	1.158	24.88	80.16	23.08	3.11
		forward	1.146	24.78	78.76	22.37	
	30 mM	reverse	1.145	24.52	78.07	21.92	3.96
		forward	1.131	24.41	76.24	21.05	
PPAI	12 mM	reverse	1.168	25.05	81.59	23.87	1.41
		forward	1.163	25.03	80.79	23.52	
	20 mM	reverse	1.156	24.94	80.77	23.29	1.74
		forward	1.148	24.93	79.98	22.89	
	30 mM	reverse	1.150	24.80	78.85	22.49	2.45
		forward	1.141	24.74	77.71	21.94	
PBAI	12 mM	reverse	1.170	24.86	80.66	23.46	1.47
		forward	1.166	24.82	79.92	23.13	
	20 mM	reverse	1.164	24.74	80.23	23.10	1.67
		forward	1.156	24.72	79.54	22.73	
	30 mM	reverse	1.157	24.50	78.05	22.12	2.16
		forward	1.149	24.46	77.03	21.65	

Table S5. The high-resolution XPS data of Ag 3d and I 3d peaks of the samples, which are extracted from Avantage analysis software.

Sample	Peak	Height (CPS)	FWHM (eV)	Area P (CPS·eV)	Area N (KE^0.6)	Sensitivity factor	Atomic (%)
control	Ag $3d_{5/2}$	1224107.08	0.73	1230810.78	824.27	22.131	51.68
	Ag $3d_{3/2}$	847892.16	0.71	880927.63	591.86	22.131	37.11
	I $3d_{5/2}$	126328.38	1.09	298008.69	121.28	42.416	7.60
	I $3d_{3/2}$	85135.34	1.09	140237.92	57.53	42.416	3.61
PMAI	Ag $3d_{5/2}$	1238381.69	0.73	1232752.96	825.65	22.131	53.22
	Ag $3d_{3/2}$	859381.36	0.70	880278.12	591.48	22.131	38.13
	I $3d_{5/2}$	109796.80	1.07	213190.94	86.77	42.416	5.59
	I $3d_{3/2}$	74176.61	1.08	115840.19	47.52	42.416	3.06
PEAI	Ag $3d_{5/2}$	1276235.23	0.73	1277104.21	855.37	22.131	53.30
	Ag $3d_{3/2}$	885590.59	0.70	912060.99	612.85	22.131	38.19
	I $3d_{5/2}$	110824.11	1.14	209978.71	85.46	42.416	5.33
	I $3d_{3/2}$	75489.97	1.13	124482.26	51.07	42.416	3.18
PPAI	Ag $3d_{5/2}$	1425026.10	0.69	1382903.02	926.24	22.131	53.99
	Ag $3d_{3/2}$	959734.90	0.70	993576.95	667.62	22.131	38.91
	I $3d_{5/2}$	91381.26	1.12	197343.46	80.32	42.416	4.68
	I $3d_{3/2}$	62087.58	1.10	101069.71	41.47	42.416	2.42
PBAI	Ag $3d_{5/2}$	1366212.17	0.73	1366703.19	915.44	22.131	54.20
	Ag $3d_{3/2}$	947593.36	0.70	978853.85	657.77	22.131	38.95
	I $3d_{5/2}$	86833.35	1.11	190127.36	77.39	42.416	4.58
	I $3d_{3/2}$	58560.35	1.08	93243.76	38.26	42.416	2.27

Table S6. SCLC parameters of the hole-only and electron-only devices.

Device	Type	V_{TFL} (V)	N_t (cm^{-3})
control	hole-only	0.435	1.39×10^{15}
	electron-only	0.536	1.72×10^{15}
PMAI	hole-only	0.308	9.86×10^{14}
	electron-only	0.478	1.53×10^{15}
PEAI	hole-only	0.214	6.85×10^{14}
	electron-only	0.344	1.10×10^{15}
PPAI	hole-only	0.166	5.31×10^{14}
	electron-only	0.263	8.42×10^{14}
PBAI	hole-only	0.164	5.25×10^{14}
	electron-only	0.161	5.15×10^{14}

Reference

1. S. Tan, I. Yavuz, M. H. Weber, T. Huang, C.-H. Chen, R. Wang, H.-C. Wang, J. H. Ko, S. Nuryyeva, J. Xue, Y. Zhao, K.-H. Wei, J.-W. Lee and Y. Yang, *Joule*, 2020, **4**, 2426-2442.
2. W. S. Yang, B.-W. Park, E. H. Jung, N. J. Jeon, Y. C. Kim, D. U. Lee, S. S. Shin, J. Seo, E. K. Kim, J. H. Noh and S. I. Seok, *Science*, 2017, **356**, 1376-1379.
3. Y. Zhao, F. Ma, Z. Qu, S. Yu, T. Shen, H.-X. Deng, X. Chu, X. Peng, Y. Yuan, X. Zhang and J. You, *Science*, 2022, **377**, 531-534.
4. Q. Jiang, Y. Zhao, X. Zhang, X. Yang, Y. Chen, Z. Chu, Q. Ye, X. Li, Z. Yin and J. You, *Nat. Photonics*, 2019, **13**, 460-466.
5. R. A. Awni, Z. Song, C. Chen, C. Li, C. Wang, M. A. Razooqi, L. Chen, X. Wang, R. J. Ellingson, J. V. Li and Y. Yan, *Joule*, 2020, **4**, 644-657.
6. C. Chen, Z. Song, C. Xiao, R. A. Awni, C. Yao, N. Shrestha, C. Li, S. S. Bista, Y. Zhang, L. Chen, R. J. Ellingson, C.-S. Jiang, M. Al-Jassim, G. Fang and Y. Yan, *ACS Energy Letters*, 2020, **5**, 2560-2568.
7. X. Fu, T. He, S. Zhang, X. Lei, Y. Jiang, D. Wang, P. Sun, D. Zhao, H.-Y. Hsu, X. Li, M. Wang and M. Yuan, *Chem*, 2021, **7**, 3131-3143.
8. C. Liu, D. Zhang, Z. Li, X. Zhang, L. Shen and W. Guo, *Adv. Funct. Mater.*, 2018, **28**, 1803126.
9. T. Walter, R. Herberholz, C. Müller and H. W. Schock, *J. Appl. Phys.*, 1996, **80**, 4411-4420.
10. S. S. Hegedus and E. A. Fagen, *J. Appl. Phys.*, 1992, **71**, 5941-5951.
11. R. Lin, J. Xu, M. Wei, Y. Wang, Z. Qin, Z. Liu, J. Wu, K. Xiao, B. Chen, S. M. Park, G. Chen, H. R. Atapattu, K. R. Graham, J. Xu, J. Zhu, L. Li, C. Zhang, E. H. Sargent and H. Tan, *Nature*, 2022, **603**, 73-78.
12. Q. Cheng, H. Xia, X. Li, B. Wang, Y. Li, X. Zhang, H. Zhang, Y. Zhang and H. Zhou, *Solar RRL*, 2022, **6**, 2100805.